AJNR

CT and MR Imaging after Placement of the GliaSite Radiation Therapy System to Treat Brain Tumor: Initial Experience

Maria G. Matheus, Mauricio Castillo, Matthew Ewend, Jeffrey K. Smith, Lester Knock, Sharon Cush and David E. Morris

AJNR Am J Neuroradiol 2004, 25 (7) 1211-1217
http://www.ajnr.org/content/25/7/1211

CT and MR Imaging after Placement of the GliaSite Radiation Therapy System to Treat Brain Tumor: Initial Experience

Maria G. Matheus, Mauricio Castillo, Matthew Ewend, Jeffrey K. Smith, Lester Knock, Sharon Cush, and David E. Morris

BACKGROUND AND PURPOSE: **The GliaSite system delivers local, high radiation after brain tumor resection. We describe the imaging appearance of the device and the changes it causes.**

METHODS: **Eight patients with brain tumors were treated with this system. After surgery, all underwent MR imaging, and one underwent CT. Five were examined 1 month after radioactive unloading and every 2 months thereafter (total, 6–9 months). Initial studies were assessed for balloon appearance and complications; subsequent studies, for signal intensity and enhancement. Three patients underwent multivoxel proton MR spectroscopy, and one underwent MR perfusion study. Spectra were reviewed for metabolites suggesting tumor; perfusion studies were reviewed for increased relative cerebral blood volume and flow.**

RESULTS: **CT showed the hyperattenuating balloon with considerable artifact. All MR images showed the device and adjacent brain. Follow-up studies showed enhancement and T2 hyperintensity in five patients. In one, enhancement progressively disappeared with no evidence of tumor recurrence. Another patient had progressive enhancement and low relative cerebral blood volume and flow; biopsy showed necrosis and inflammation. One patient had progressive enhancement and high choline levels (proved anaplastic astrocytoma). In another, T2 signal intensity and contrast enhancement progressed owing to tumor and bacterial infection. The last patient had a high choline level (proved radionecrosis); enhancement progressed over 5 months. In three, the device was removed early because of bleeding, mass effect, and therapeutic changes (no follow-up).**

CONCLUSION: **Good balloon visualization was possible with MR imaging. After brachytherapy, all patients developed T2 hyperintensity; stable or progressive enhancement occurred with tumor recurrence and radionecrosis. High choline levels were suggestive of, but not necessarily diagnostic of, tumor.**

Surgery and irradiation are standard treatments for primary and metastatic brain tumors. Tumor resection followed by conformal external-beam irradiation may improve the patient's survival and quality of life (1–4). Despite irradiation and other forms of therapy, brain tumors recur at or near the surgical bed (5). The aim of combined therapy is to sterilize the resection bed and limit injury to normal adjacent tissues; however, avoiding injury to adjacent tissues can be difficult. By distributing radiation to the tumor bed and to only the most immediate surrounding tissues, brachytherapy may reduce radiation injury.

The GliaSite radiation therapy system (GSRTS) is a new brain brachytherapy applicator (Proxima Therapeutics, Alpharetta, GA). This device comprises an inflatable balloon connected to an infusion port by a multilumen, silicone catheter shaft designed to deliver an intracavitary single, large dose of ionizing radiation at a low rate (6, 7). After tumor resection, a catheter is placed in the resection bed, the balloon is inflated with iodinated contrast agent, and its position is checked with CT or MR imaging or both. If its position is adequate, it is loaded with sodium 3-[^{125}I]iodo-4-hydroxybenzenesulfonate (Iotrex; Proxima Therapeutics, Inc., Alpharetta, GA) in sodium chloride solution. Delivered doses are in the range of 40–60 Gy at

Received September 30, 2003; accepted after revision December 22.

From the Departments of Radiology (M.G.M., M.C., J.K.S., L.K.), Neurosurgery (M.E., S.C.) and Radiation Oncology (D.E.M.), University of North Carolina School of Medicine, Chapel Hill.

Address reprint requests to Mauricio Castillo, MD, Department of Radiology, University of North Carolina, Chapel Hill, NC 27599.

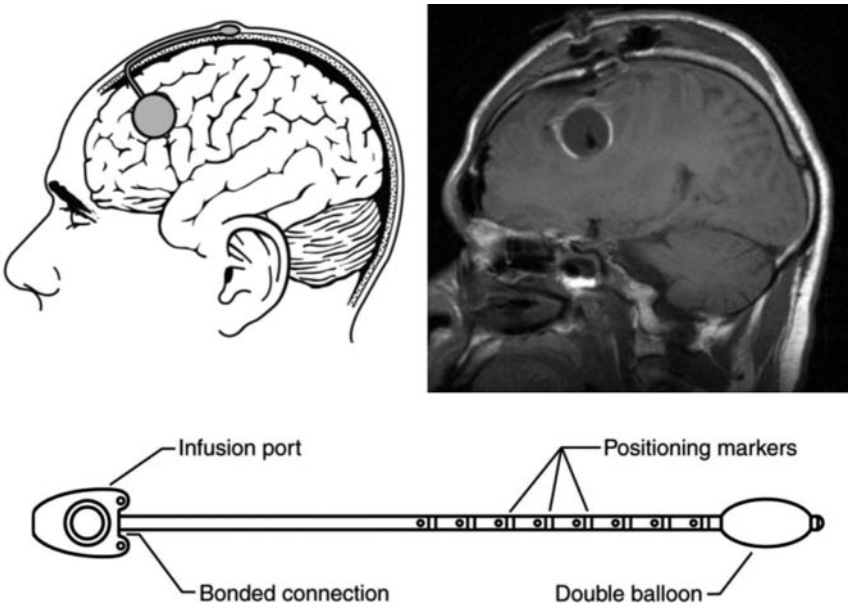

FIG 1. GSRTS device. *Upper left*, Diagram shows the balloon, subcutaneous tube, and port. *Upper right*, Corresponding sagittal nonenhanced T1-weighted MR image (TR/TE/NEX = 500/12/1) obtained 24 hours after tumor resection and implantation shows the balloon surrounded by a thin, hyperintense peripheral zone corresponding to a thin layer of blood. Central hypointense area corresponds to the tube. Visualization of neighboring tissues is good. *Bottom*, Diagram shows components of the device.

rates of 40–60 cGy/h and at depths of 0.5–1.0 cm from the surface of the balloon. Thus, the device provides a homogeneously high dose to the edges of the resection, with relative sparing of the neighboring tissues (8, 9).

We describe our preliminary experience with CT and MR imaging for the assessment of balloon conformance, its complications, and the parenchymal changes induced by the treatment.

Methods

We retrospectively reviewed all CT and MR imaging studies acquired in eight patients who underwent surgical resection of brain tumors and implantation of GSRTS into the tumor beds (Fig 1). The patients included six men and two women aged 52–75 years (mean, 65 years). All patients underwent preoperative contrast-enhanced MR imaging. Eight underwent contrast-enhanced MR imaging, and one underwent contrast-enhanced CT less than 48 hours after placement of the device.

In all patients, gross tumor resection and GSRTS placement were preformed during the same surgery. In the operating room, after the tumor was debulked, the remaining cavity was measured with a Foley catheter. On the basis of the catheter volume, a GSRTS of one of the three available sizes (2-, 3-, or 4-cm balloon diameter) was chosen. The device was loaded with diluted iodinated contrast agent, and its position and configuration was assessed immediately with frontal and lateral radiographs. Within 48 hours of surgery, CT or MR imaging was performed to assess the position and configuration of the device. At 7–15 days after surgery, the contrast material inside the balloons was removed, and the balloons were loaded with a precalculated dose of Iotrex. The radioactive material remained inside the device for 99.7–123.9 hours, depending on the size of the device; in our group, the average was 111.6 hours. The aim of this procedure was to obtain 60 Gy absorbance at 1.0 cm from the surface of the balloon in accordance with protocols established in the GliaSite clinical trial (8, 9). After this period, the devices were removed, and because all patients were clinically stable, no immediate imaging was performed.

The first follow-up study was obtained 1 month after radioactive unloading. Five patients underwent radioactive balloon loading and underwent follow-up contrast-enhanced MR imaging 1 month after radioactive unloading of the balloon and then at 2-month intervals for 6–9 months. In three patients, the device was removed before radioactive loading because of concurrent clinical problems and changes in therapeutic approach.

CT study included 5-mm-thick sections before and after the intravenous administration of contrast material. All MR imaging studies were performed by using 1.5-T units (Magneton Sonata; Siemens Medical Systems, Erlangen, Germany) with circular polarized-head coils, and consisted of the following: 1) 5-mm-thick, sagittal T1-weighted images (TR/TE/NEX = 500/20/1); 2) 5-mm-thick, fast spin-echo axial T2-weighted images (5050/99/1, echo train length = 11); 3) 4-mm-thick, axial fast fluid-attenuated inversion recovery (FLAIR) images (8000/110/1, inversion time = 2500, echo train length = 11); 4) 5-mm-thick axial trace diffusion-weighted images (180/122/6; b = 10, 500, and 1000 s/mm^2) and corresponding apparent diffusion coefficient maps; 5) 1.5-mm-thick, axial gradient recalled-echo, 3D T1-weighted images (3.5/7/1) before and after intravenous gadolinium enhancement; and 6) contrast-enhanced, 5-mm-thick, coronal T1-weighted images (500/12/1). Initial and follow-up studies were obtained with identical protocols.

Proton MR spectroscopy was performed in three patients 5 months after radioactive loading. This was accomplished by using a multivoxel 2D chemical-shift point-resolved technique after the water peak was suppressed by a chemical-shift selective excitation. Localization of the region to be examined with MR spectroscopy was determined from the contrast-enhanced T1-weighted images and after the studies were shimmed by using short and long TEs of 30 and 135 milliseconds (TR = 1500 ms). The individual voxels varied from 0.5 × 0.5 × 1.5 to 1.0 × 1.0 × 1.5 cm, depending on the size of the enhancing regions. Each voxel was processed by using an exponential filter of 4 Hz and manually phased. The baselines were corrected for each voxel by using a polynomial function and the curve-fitting software provided by the vendor.

MR perfusion study was performed in one patient 7 months after radioactive loading. The study included 20 sections at 5.0-mm thickness (20% gap) and was done by using a multishot gradient-echo echo-planar sequence (echo-planar imaging factor = 64). Forty measurements were done in 1.24 minutes (TR/TE = 2000/54, flip angle = 60°) by using a 128 × 128 matrix and a 230-mm field of view. The images were obtained during the first pass of a 0.1-mmol/kg bolus of gadolinium-based contrast agent administered at a rate of 4 mL/s by using

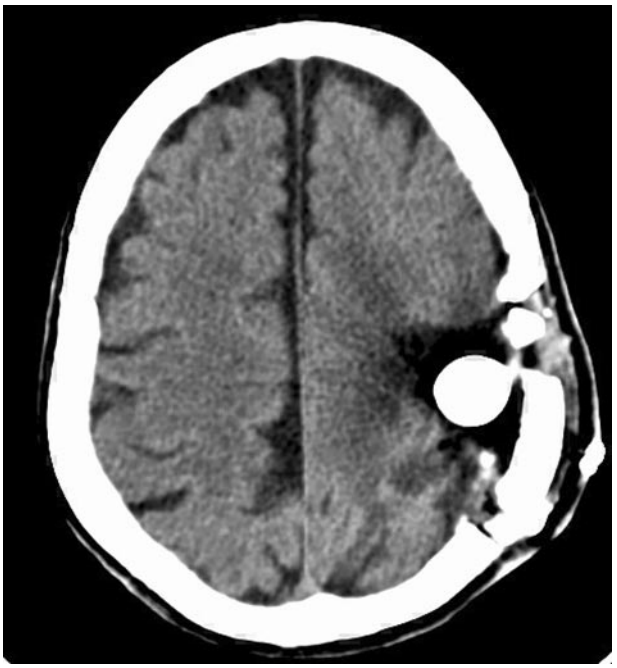

FIG 2. CT scan obtained <48 hours after device implantation shows the attenuating balloon filled with iodinated contrast material, with artifacts obscuring tissues around it.

a power injector. Postprocessing of the images was done with proprietary software that calculated the relative cerebral blood flow (rCBF), relative cerebral blood volume (rCBV), mean transient time (MTT), and time to peak (TTP). The arterial input function used for the singular value decomposition was selected on the basis of voxels from the middle cerebral artery.

Two neuroradiologists (M.C., J.K.S.) reviewed all imaging studies. Studies performed less than 48 hours after tumor resection and device implantation were reviewed with attention to the morphology of the GSRTS and the appearance of the surrounding brain parenchyma. The conformance of the catheters was assessed by measuring the distance between the balloon surface and surrounding brain parenchyma with the digital calipers; distances greater than 1.0 cm were considered to be a lack of conformance. Subsequent follow-up studies were assessed for changes in contrast enhancement and signal intensity in the brain parenchyma neighboring the resection site, with special attention to changes in these parameters throughout the follow-up period. MR spectroscopic studies were reviewed with attention to elevation of the choline (Cho) peak, which suggested the presence of tumor. The perfusion study was assessed for elevated rCBV and rCBF.

Results

The tumors were located in the left frontotemporal region ($n = 4$), right frontotemporal region ($n = 3$), and right parietal lobe ($n = 1$). They measured 2.0–3.5 cm in greatest dimension. Three patients had primary brain tumors (glioblastoma multiforme in two, anaplastic astrocytoma in one), and five patients had single brain metastases (non–small cell lung cancer in two, lung squamous cell carcinomas in two, and small cell lung cancer in one).

In all patients, the GSRTS device was clearly identified. The balloon was hyperattenuated on CT scans (Fig 2), reflecting the iodinated contrast material. It had low signal intensity on T1-weighted and FLAIR MR images and high signal intensity on T2-weighted MR images (Fig 3). On one CT study, the brain immediately around the balloon could not be seen because of artifacts (Fig 2). On all MR imaging studies, the brain adjacent to the balloons was well depicted with all sequences (Fig 3).

In three patients, the catheters removed in the early postoperative period. One patient had acute postoperative hyponatremia (sodium level = 129 mmol/L), followed by brain edema and bleeding requiring an emergency craniotomy for decompression. In another patient, the device was removed because of substantial bleeding around it; this was the result of anticoagulation therapy for bilateral deep venous thrombosis and pulmonary embolus. In the third patient, the catheter was removed because of a change in the therapeutic approach and a lack of catheter conformance. A small amount of blood was present inside the surgical bed, but the distance between the balloon surface and target tissue was more than 1.0 cm; this finding was considered a lack of conformance (Fig 4). None of these three patients had follow-up studies.

After contrast enhancement administration, all MR images obtained at 1-month follow-up demonstrated enhancement along the resection borders. The pattern of enhancement varied from thin and rimlike to inhomogeneous, thick, and somewhat nodular. Five patients underwent MR imaging 1 month after radioactive unloading of the device. (Two patients had a glioblastoma multiforme; one, anaplastic astrocytoma; one, squamous cell carcinoma; and one, non–small cell lung cancer.) At the time of this report, all devices had been removed (10 months after the beginning of the trial). Studies were then obtained every 2 months for the duration of follow-up (9 months in three patients, 6 months in two).

We observed high T2 signal intensity in the tissues around the balloons in all patients 1 month after radioactive unloading. The borders of this high signal intensity were initially poorly defined but became better defined after 3 months. In three patients, this area of high signal intensity had no mass effect and remained stable in size and distribution for the entire duration of follow-up. In one of these patients (who had a metastasis), the initial contrast enhancement progressively disappeared, and 9 months after radioactive loading, she was considered to be in stable condition and free of obvious disease. Another one had progressive focal enhancement along the edges of the balloon, and the MR perfusion study demonstrated low rCVB and rCBF in this region (Fig 5). In this same patient, MR spectroscopy showed high levels of Cho and low levels of *N*-acetyl-aspartate (NAA). Because of the discrepancy between MR imaging and perfusion studies, the patient underwent biopsy of this region, which demonstrated only inflammatory reactive changes and necrosis. The third patient in this group showed progressive contrast enhancement around the resection, and MR spectroscopy of this area showed high Cho levels, low NAA levels, and the presence of macrolipids (Fig 6). Biopsy of this region showed anaplastic astrocytoma. During

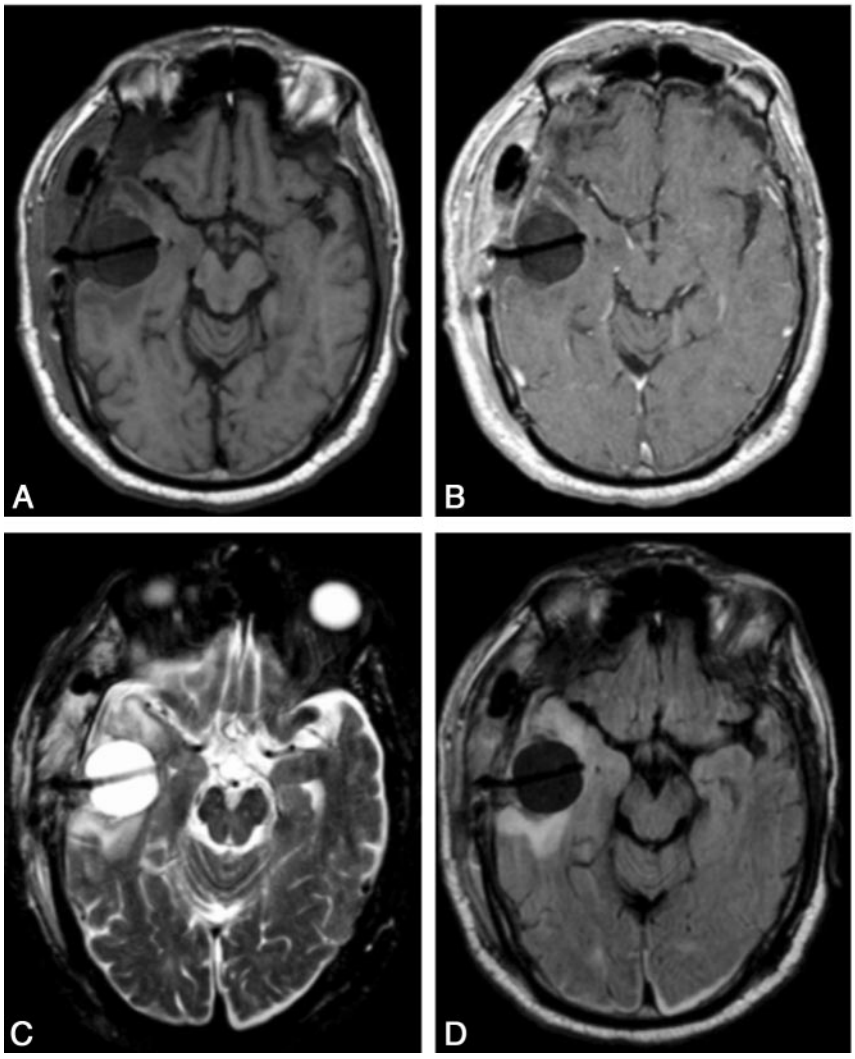

FIG 3. MR images obtained <48 hours after surgery.

A, Axial nonenhanced T1-weighted image (500/12/1) shows the hypointense balloon and central shaft (tube), with good visualization of surrounding tissues.

B, Axial contrast-enhanced T1-weighted image (500/12/1) shows the well-defined borders of the device and surrounding tissue, associated with thin enhancement of the surgical bed.

C, Corresponding axial T2-weighted image (5050/99/1) shows the hyperintense balloon. There is a small amount of ill-defined hyperintensity in adjacent tissues.

D, Corresponding axial FLAIR image (8000/110/1) shows the hyperintensity in the tissues around the balloon better. These areas are most likely residual vasogenic tumor edema and postsurgical changes.

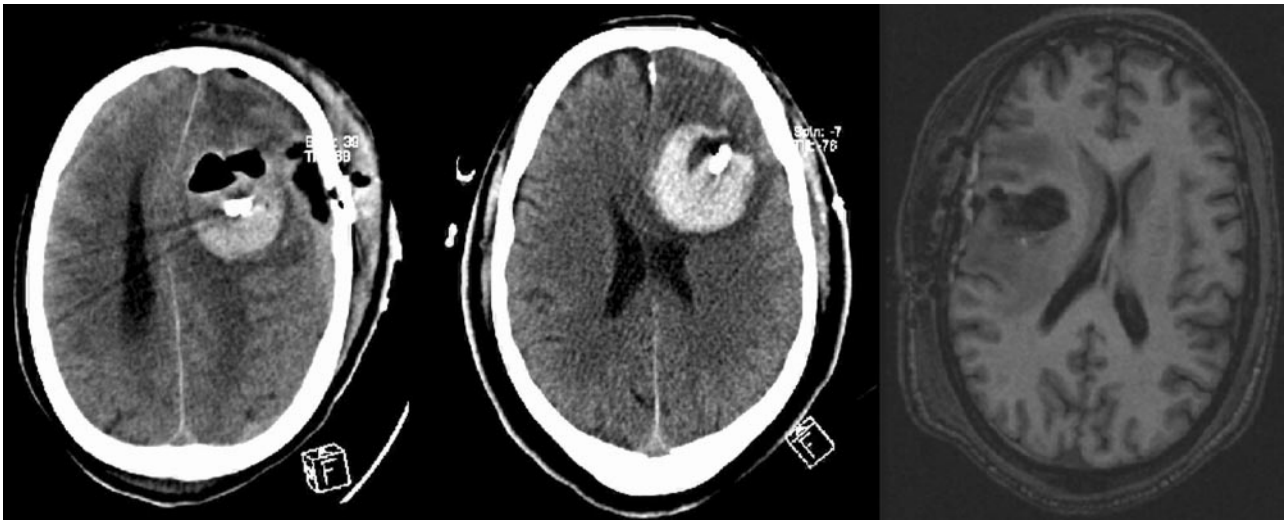

FIG 4. Images from the three patients in whom the devices were removed before radioactive unloading. *Left*, CT scan shows mass effect and bleeding around the device after acute hyponatremia. *Center*, CT scan shows substantial hemorrhage in the surgical cavity in this patient with coagulopathy. *Right*, 3D gradient-echo T1-weighted image (3.5/7/1) shows blood products in the surgical cavity and an increased distance between the edges of the balloon and surrounding tissues; this was considered a lack of conformance.

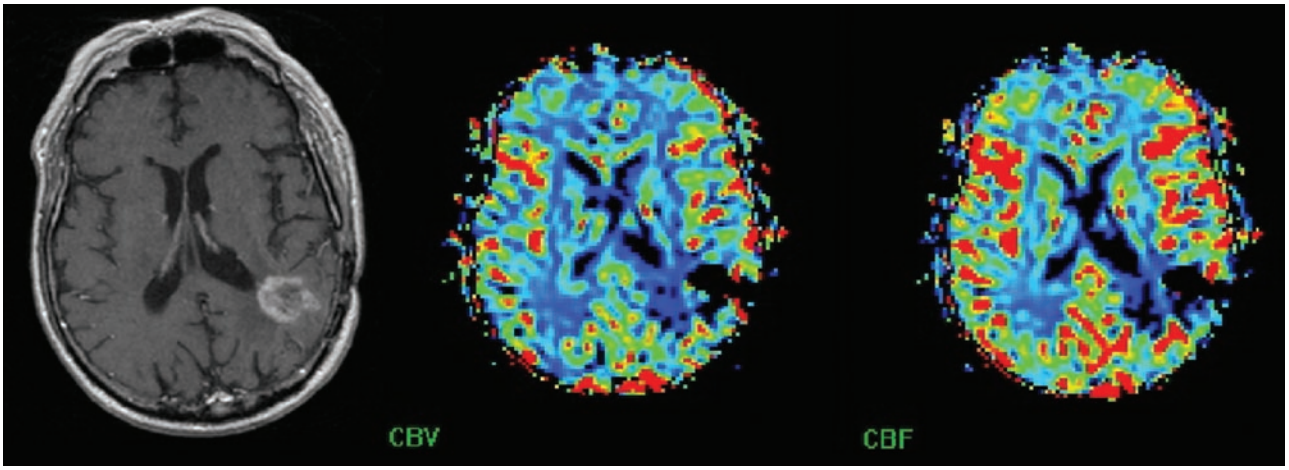

FIG 5. Perfusion maps after device removal in a patient treated for a brain metastasis. *Left*, Axial contrast-enhanced T1-weighted image (500/12/1) shows an irregular ringlike area of enhancement at the resection site. *Center* and *right*, Color perfusion maps show low rCBV and rCBF in the site of the lesion. At biopsy, no tumor was found.

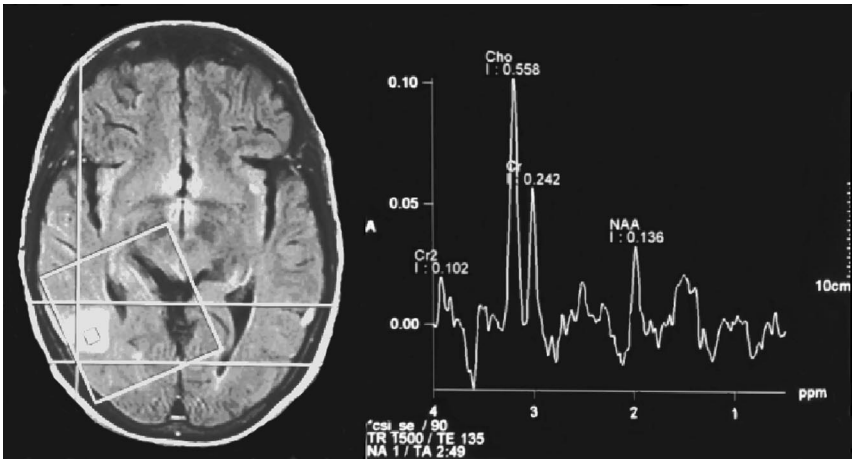

FIG 6. Results of MR spectroscopy after the device was removed in the treatment of anaplastic astrocytoma. *Left*, Axial contrast-enhanced T1-weighted localizer image shows the voxel. *Right*, Long-TE (135-ms) spectrum from the voxel shows an elevated Cho peak and a low NAA level.

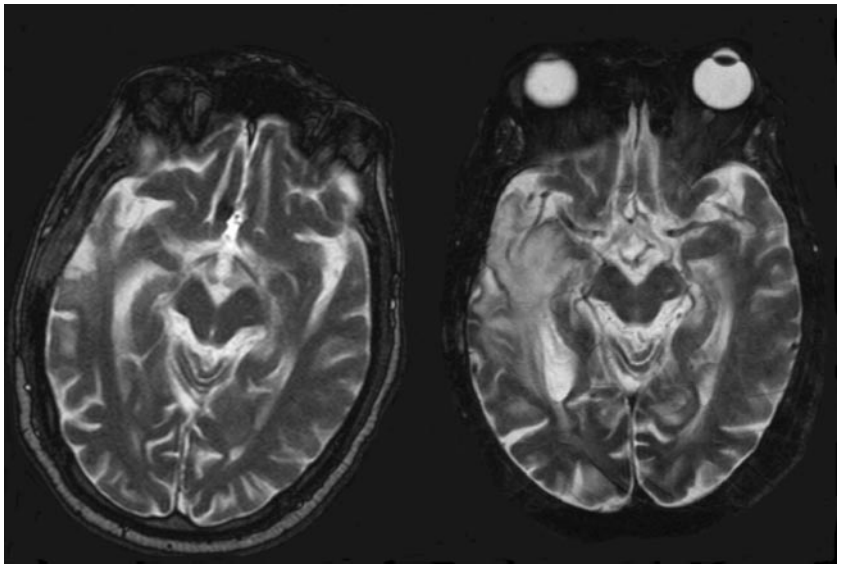

FIG 7. Progressive signal-intensity abnormality after device removal. *Left*, Axial T2-weighted image (5050/99/1) at 1 month after removal shows minimal, somewhat ill-defined, hyperintensity in the right temporal lobe. *Right*, Corresponding axial T2-weighted image (5050/99/1) 5 months later shows progressive hyperintensity and mass effect; however, only radionecrosis was found at pathologic analysis.

6-month follow-up, the fourth patient had progressive high T2 signal intensity, mass effect, and contrast enhancement around the balloon. Biopsy confirmed residual tumor (glioblastoma multiforme) and superimposed multibacterial infection. In the last patient, progressively increased T2 signal intensity, mass effect, and contrast enhancement around the resection were noted. MR spectroscopy showed high Cho levels, low NAA levels, and areas of contrast enhancement, but multiple biopsy procedures revealed only

radionecrosis (Fig 7). Diffusion-weighted images did not offer additional information in any patient.

Discussion

The GSRTS device aims to deliver a high homogeneous radioactive dose to tissues within a short distance. At a distance greater than 1.0 cm from the balloon surface, the dose decreases in an exponential fashion (9). Therefore, the imaging methods used to assess the position of the device should be able to clearly show the edges of the balloon and the surrounding areas. Our results demonstrated a typical appearance of the catheter with all imaging techniques that permits its identification and confirmation of its position. On CT scans, artifacts related to the high attenuation of iodated contrast agent inside the balloon catheter obscured the surrounding tissues; therefore, we believe that MR imaging is a better method for the initial examination of these patients. Alternatively, a lower concentration of iodinated contrast material (higher dilution in saline solution) could be used (10, 11). Immediately after surgery, it is important to exclude complications such as hemorrhage and to assess how the balloon conforms to the surgical cavity. Conformation of the balloon to the edges of the resection is also desirable to ensure a uniform delivery of radiation. Lack of conformation may affect the uniform delivery of radiation. The silicon walls of the balloon lack signal intensity at MR imaging, and this feature permits their identification. It is conceivable that a balloon may also burst, spilling its contents into the resection bed. This occurrence has not been reported and is presumably unlikely, because the balloon has double walls. Conversely, blood products of different ages and CSF might conceivably compress the balloon and simulate its rupture.

The goal in brachytherapy is the delivery of a maximum radiation dose to a tumor bed with substantially lower doses to the distant tissues (7, 8). Two factors make this approach desirable: tumor cells are more susceptible to radiation-induced injury than are normal tissues, and normal cells have a superior capacity to repair sublethal radiation damage, especially in organs formed by cells with low cellular division rates such as the brain (12). Radiation therapy promotes direct cell injury by depositing energy in a targeted area or indirect cell injury caused by free radical formation, release of inflammatory agents (eicosanoides, histamine, cyclic adenosine monophosphate), and lysozymes (12). These indirect factors amplify radiation-induced cell injury. Radiation damage is also caused by a combination of effects on endothelial and stromal cells (13). This vascular phenomenon seems to be an early and important step of radiation-induced damage and may be reflected on imaging studies. The cycling endothelium is an easy target for radiation damage associated with the release of inflammatory agents that promote brain blood–barrier breakdown, focal necrosis, and edema (9, 12, 13). Hypothetically, this may be reflected in the contrast enhancement and T2 hyperintensity seen in the images of all of our patients as early as 1 month after local delivery of the high-radiation dose. At this point, distinguishing between residual tumor and hyperacute radiation is not feasible with MR imaging alone.

In our patients, progressive hyperintense abnormalities on T2-weighted images were due to tumor recurrence (plus infection in one patient) or radiation-induced necrosis. In one patient with stable T2 abnormalities throughout follow-up, no obvious tumor or necrosis developed. Similarly, a change in the pattern of contrast enhancement was also correlated with the development of radiation-induced necrosis or the presence of a tumor. Tumors or necrosis failed to develop in only the patient with a progressive decline in contrast enhancement.

Functional imaging methods such as MR spectroscopy and perfusion study may aid in the diagnosis of brain tumors when combined with conventional MR imaging. High levels of Cho are seen in tumors (14, 15). Associated high levels of *myo*-inositol may suggest reactive changes and gliosis (14, 15). Our MR spectroscopic results were variable. One patient with high Cho levels had tumor recurrence. One patient also had a pyogenic infection in the same areas as the tumor. Cho is a marker of high cellular proliferation and turnover, and its level is elevated in brain tumors and infectious or inflammatory processes (16, 17). In another patient, the Cho level was high, but repeat resection showed only necrosis. We believe that the presence of inflammatory cells related to hyperacute radiation damage to the tissue may explain the high Cho levels in this patient (16, 17).

MR perfusion study was performed in only one patient and showed low rCBV and rCBF in the area of contrast enhancement. Biopsy of this area showed no tumor recurrence. Previous publications report that radionecrosis has decreased rCBV, whereas tumors have increased rCBV (18, 19). In our patient, the finding of the low perfusion and contrast enhancement in the same area is perhaps related to a vascular-flaring reaction and to breakdown of the blood-brain barrier, which has been observed after brachytherapy (2, 3, 9).

The present findings should be interpreted with caution and as preliminary because of the small number of patients. Although conventional MR imaging findings are known to be nonspecific for differentiating tumor from radiation-induced effects, the accuracy of MR spectroscopy and perfusion has not been assessed in the setting of intense brachytherapy. Our results may help in organizing follow-up imaging protocols in these patients and in guiding therapy; however, they should be confirmed in a larger number of patients. In addition, our purpose was to describe the imaging findings after GSRTS implantation and not to evaluate the effectiveness of this treatment.

Conclusion

We found that visualization of the GSRTS balloon and surrounding tissues was better with MR imaging than with CT. MR imaging provided important infor-

mation in the immediate postoperative period leading to device removal in three patients whose images showed hemorrhage, mass effect related to concurrent clinical complications, and lack of device conformance. In all patients in whom the device was radioactively loaded, surrounding T2 hyperintensity and progressive contrast enhancement developed with both tumor recurrence and radionecrosis. High Cho levels at MR spectroscopy were suggestive but not diagnostic of tumor. In one patient, lack of increased rCBF and rCBV at perfusion MR imaging was correlated with an absence of tumor despite progressive contrast enhancement in the same region.

References

1. Gaspa L, Scott C, Rotman M, et al. **Recursive Partitioning Analysis (RPA) of prognostic factors in three Radiation Therapy Oncology Group (RTOG) brain metastases trials.** *Int J Radiation Oncology Biol Phys* 1997;37:745–751
2. McDermott MW, Cosgrove GR, Larson DA, et al. **Interstitial brachytherapy for intracranial metastases.** *Neurosurgery Clinics of North America.* 1996;7:485–495
3. Sneed PK, Larson AD, Wara WM. **Radiotherapy for cerebral metastases.** *Neurosurg Clin N Am* 1996;7:505–515
4. Heros DO, Ksdon DL, Chun M. **Brachytherapy in treatment of recurrent solitary brain metastases.** *Neurosurgery* 1988;23:733–737
5. Sneed PK, Gutin PH, Larson DA, et al. **Patterns of recurrence of Glioblastoma Multiforme after external irradiation followed by implant boost.** *Int J Radiat Oncol Biol Phys* 1994;29:719–727
6. Stubbs JB, Strickland AD, Frank RK, et al. **Biodistribution and dosimetry of an aqueous solution containing sodium3-(125 I)iodo-4-hydroxybenzenesulfonate (Iotrex TM) for brachytherapy of resected malignant brain tumors.** *Cancer Biother Radiopharm* 2000;15:645–656
7. Monroe JI, Dempsey JF, Dorton JA, et al. **Experimental validation of dose calculation algorithms for GliaSite TM RTS, a novel 125 I liquid-filled balloon brachytherapy applicator.** *Med Phys* 2001;28:73–85
8. Tatter SB, Shaw EG, Rosenblum ML, et al. **An inflatable balloon catheter and liquid 125I radiation source (GliaSite Radiation Therapy System) for treatment of recurrent malignant gliomas: multicenter safety and feasibility trial.** *J Neurosurg* 2003;99:297–303
9. Stubbs JB, Frankel RH, Schultz K, et al. **Preclinical evaluation of a novel device delivering brachytherapy to the margins of resected brain tumor cavities.** *J Neurosurg* 2002;96:335–343
10. deGuzman AF, Karvelis KC, Shaw EG, et al. **Brachytherapy of re-resected malignant gliomas cavity margins using an inflatable balloon catheter and a liquid I-125 source: a phase I study [abstract].** Presented at the 47th Annual Meeting of the Society of Nuclear Medicine, St Louis, June 3–7, 2000
11. Dame EA, Putzer GJB, Pearlman JL, et al. **Imaging appearance of a new radiation therapy delivery device for CNS tumors.** *AJNR Am J Neuroradiol* 2001;22:1806–1807
12. Leibel SA, Gutin PH, Davis RL. **Factors affecting radiation injury after interstitial brachytherapy.** In: Gutin PH, Leibel SA, Sheile GE, eds. *Radiation Injury to the Nervous System.* New York: Raven Press; 1991:257–263
13. Philips TL. **Early and late effects of radiation on normal tissues.** In: Gutin PH, Leibel SA, Sheile GE, eds. *Radiation Injury to the Nervous System.* New York: Raven Press; 1991:37–50
14. Esteve F, Rubin C, Grand S, et al. **Transient metabolic changes observed with proton MR spectroscopy in normal human brain after radiation therapy.** *Int J Radiation Oncology Biol Phys* 1998;40:279–286
15. Chan Y, Yeung DKW, Leung S, et al. **Proton magnetic resonance spectroscopy of late delayed radiation-induced injury of the brain.** *J Magn Reson Imaging* 1999;10:130–137
16. Cecil KM, Lenkinski RE. **Proton MR spectroscopy in inflammatory and infectious brain disorders.** *Neuroimaging Clin N Am 1998;8:863–880*
17. Inglese M, Li BSY, Rusinek H, et al. **Diffusely elevated cerebral choline and creatine in relapsing-remitting multiple sclerosis.** *Magn Reson Med* 2003;50:190–195
18. Sugahara T, Korogi Y, Tomiguchi S, et al. **Posttherapeutic intraaxial brain tumor: the value of perfusion-sensitive contrast-enhanced MR Imaging for differentiating tumor recurrence from nonneoplastic contrast-enhancing tissue.** *AJNR Am J Neuroradiol* 2000;21:901–909
19. Aksoy FG, Lev MH. **Dynamic contrast-enhanced brain perfusion imaging technique and clinical applications.** *Semin Ultrasound CT MR.* 2000;21:462–477